

## Molecular Basis for Omapatrilat and Sampatrilat Binding to Neprilysin—Implications for Dual Inhibitor Design with Angiotensin-Converting Enzyme

Urvashi Sharma,<sup>§</sup> Gyles E. Cozier,<sup>§</sup> Edward D. Sturrock, and K. Ravi Acharya\*Cite This: *J. Med. Chem.* 2020, 63, 5488–5500

Read Online

ACCESS |



Metrics &amp; More



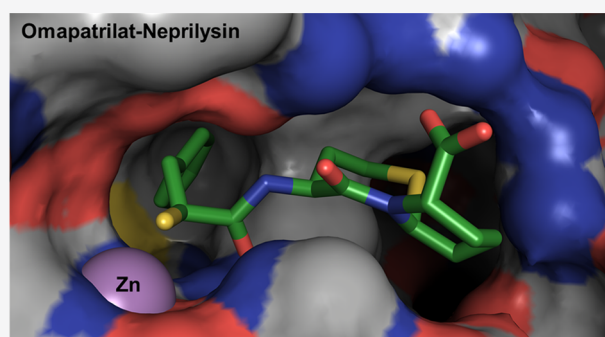
Article Recommendations



Supporting Information

**ABSTRACT:** Neprilysin (NEP) and angiotensin-converting enzyme (ACE) are two key zinc-dependent metalloproteases in the natriuretic peptide and kinin systems and renin–angiotensin–aldosterone system, respectively. They play an important role in blood pressure regulation and reducing the risk of heart failure. Vasopeptidase inhibitors omapatrilat and sampatrilat possess dual activity against these enzymes by blocking the ACE-dependent conversion of angiotensin I to the potent vasoconstrictor angiotensin II while simultaneously halting the NEP-dependent degradation of vasodilator atrial natriuretic peptide. Here, we report crystal structures of omapatrilat, sampatrilat, and sampatrilat-ASP (a sampatrilat analogue) in complex with NEP at 1.75, 2.65, and 2.6 Å, respectively.

A detailed analysis of these structures and the corresponding structures of ACE with these inhibitors has provided the molecular basis of dual inhibitor recognition involving the catalytic site in both enzymes. This new information will be very useful in the design of safer and more selective vasopeptidase inhibitors of NEP and ACE for effective treatment in hypertension and heart failure.



## INTRODUCTION

Cardiovascular disease (CVD) is responsible for ~30% of all deaths worldwide, most of which occur in developing countries. Hypertension is the main risk factor for CVD, and despite the large number of drugs on the market for treating hypertension, the global CVD burden continues to rise.<sup>1</sup>

In addition, many patients receiving treatment suffer from severe side effects such as angioedema and persistent cough and still eventually develop nephropathy, retinopathy, and heart failure.<sup>2–4</sup> The renin-angiotensin-aldosterone system (RAAS), the endothelin system (ES), and the natriuretic peptides and kinin system (NPKS) play important roles in blood pressure regulation; thus, peptidases and receptors within these systems are important drug targets for the treatment of hypertension.<sup>5</sup>

Single drugs targeting both angiotensin-converting enzyme (ACE, EC 3.4.15.1) and neprilysin (NEP, EC 3.4.24.11), key zinc-dependent metalloproteases in RAAS and NPKS, respectively, are an attractive therapeutic approach for the treatment of hypertension and have been termed vasopeptidase inhibitors.<sup>6–8</sup> The rationale behind this approach is to block the ACE-dependent conversion of angiotensin I to the potent vasoconstrictor angiotensin II while simultaneously decreasing the NEP-dependent degradation of vasodilators atrial natriuretic peptide (ANP) and B-type natriuretic peptide (BNP). NEP has a broad substrate specificity and is structurally similar

to ACE,<sup>7</sup> thereby facilitating the design of inhibitors that target both enzymes.

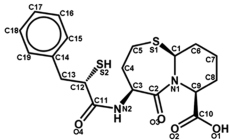
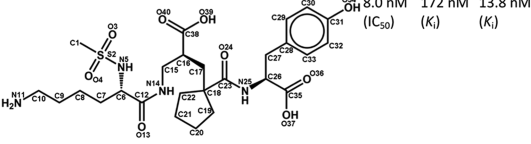
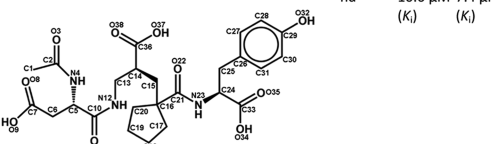
In clinical studies, omapatrilat (4*S*,7*S*,10*aS*)-5-oxo-4-[(2*S*)-3-phenyl-2-sulfanylpropanoyl]amino-2,3,4,7,8,9,10,10*a*-octahydroprido[2,1-*b*][1,3]thiazepine-7-carboxylic acid (Table 1), an extensively studied dual ACE/NEP inhibitor,<sup>9,10</sup> was highly effective at lowering blood pressure in hypertensive patients.<sup>11,12</sup> However, it also increased the incidence of the potentially fatal adverse reaction, angioedema. In addition to this, omapatrilat caused a substantial increase in the incidence of cough, flushing, and transient facial redness as well as the incidence of gastrointestinal disturbances compared to placebo. The accumulation of the vasodilator peptide bradykinin has been associated with side effects commonly observed for ACE inhibitors. Bradykinin is degraded by both ACE and NEP as well as aminopeptidase 2 (APP2), a third enzyme inhibited by omapatrilat;<sup>13</sup> as such, inhibiting these three enzymes simultaneously exacerbates the problems associated with the buildup of bradykinin. The poor safety profile of omapatrilat stalled the development of this otherwise

Received: March 16, 2020

Published: April 27, 2020



**Table 1. Structures of Inhibitors Used in This Structural Study with NEP along with Their Published Inhibition Data against NEP and the Two sACE Domains<sup>a</sup>**

Compound	Structure	NEP	nACE	cACE
Omapatrilat		8.0 nM (IC <sub>50</sub> )	2.0 nM (IC <sub>50</sub> )	1.0 nM (IC <sub>50</sub> )
Sampatrilat		8.0 nM (IC <sub>50</sub> )	172 nM (K)	13.8 nM (K)
SamASP		nd	10.6 μM (K)	7.4 μM (K)

<sup>a</sup>Inhibition data references: NEP—omapatrilat,<sup>10</sup> NEP—sampatrilat,<sup>14</sup> ACE—omapatrilat,<sup>9</sup> ACE—sampatrilat,<sup>15</sup> and ACE—samASP.<sup>15</sup>

promising class of vasopeptidase inhibitors. The C-domain (cACE) catalytic site of ACE is primarily responsible for the hydrolysis of angiotensin I. Thus, C-domain-selective inhibition allows the N-domain (nACE) catalytic site to inactivate bradykinin and decreases the potential for ACE inhibitor-induced adverse effects.<sup>5</sup>

Sampatrilat, (*S,S,S*)-*N*-{1-[2-carboxy-3-(*N*-mesylsilylamino)propyl]-1-cyclopentylcarbonyl}tyrosine (Table 1), is also a vasopeptidase inhibitor of ACE and NEP with the potential for the treatment of hypertension and congestive heart failure.<sup>16–18</sup> It is hydrophilic containing one weakly acidic phenolic (tyrosine) group, two more acidic carboxylate groups (tyrosine carboxylate and the central carboxylate), and one basic primary amine (lysine) group. Sampatrilat has a moderate 12.5-fold selectivity for cACE, whereas sampatrilat-ASP (samASP), an analogue that has an aspartate substituted for the P<sub>2</sub> lysine of sampatrilat, is nonselective.<sup>15</sup>

Lisinopril ((2*S*)-1-[(2*S*)-6-amino-2-[(1*S*)-1-carboxy-3-phenylpropyl]amino]hexanoyl]pyrrolidine-2-carboxylic acid) is a potent inhibitor of both ACE domains with a fourfold selectivity for cACE, whereas Lis-W ((2*S*)-2-[[2-[(1*R*)-1-carboxy-2-(1*H*-indol-3-yl)ethyl]amino]-1-oxohexan-2-yl]amino]-4-phenylbutanoic acid), an analogue with a P<sub>2</sub>' indole group, retains the potency for cACE, but has a 243-fold cACE selectivity.<sup>19</sup> *In vivo* studies showed that Lis-W could

**Table 2. Crystallographic Data Collection and Structure Refinement Statistics<sup>a</sup>**

	omapatrilat	sampatrilat	samASP
resolution (Å)	[93.47–9.09] (1.78–1.75)	[93.61–8.79] (2.78–2.65)	[112.96–9.01] (2.72–2.60)
space group	P3 <sub>2</sub> 21	P3 <sub>2</sub> 21	P3 <sub>2</sub> 21
cell dimensions ( <i>a</i> , <i>b</i> , <i>c</i> ) (Å)	107.94, 107.94, 112.84	108.09, 108.09, 112.83	108.17, 108.17, 112.95
angles ( $\alpha$ , $\beta$ , $\gamma$ ) (deg)	90.0, 90.0, 120.0	90.0, 90.0, 120.0	90.0, 90.0, 120.0
molecules/asymmetric unit	1	1	1
total/unique reflections	3 068 569 76 891	838 522 22 602	826 971 24 000
completeness (%)	[99.9] 100.0 (100.0)	[100.0] 100.0 (100.0)	[100.0] 100.0 (99.9)
<i>R</i> <sub>merge</sub>	[0.031] 0.137 (4.105)	[0.102] 0.472 (4.442)	[0.194] 0.587 (5.026)
<i>R</i> <sub>pim</sub>	[0.005] 0.022 (0.711)	[0.018] 0.078 (0.865)	[0.035] 0.101 (0.852)
$\langle I/\sigma(I) \rangle$	[86.2] 18.4 (1.2)	[26.1] 7.8 (1.1)	[15.3] 5.9 (1.2)
CC <sub>1/2</sub>	[1.000] 1.000 (0.507)	[0.999] 0.997 (0.535)	[0.996] 0.994 (0.546)
multiplicity	[34.4] 39.9 (34.1)	[34.9] 37.1 (26.9)	[29.2] 34.5 (35.3)
	Refinement Statistics		
<i>R</i> <sub>work</sub> / <i>R</i> <sub>free</sub>	0.166/0.200	0.191/0.238	0.208/0.254
<i>R</i> <sub>msd</sub> in bond lengths (Å)	0.003	0.003	0.002
<i>R</i> <sub>msd</sub> in bond angles (deg)	0.683	0.540	0.481
	Ramachandran Statistics (%)		
favoured	98.1	96.7	98.0
allowed	1.9	3.3	2.0
outliers	0.0	0.0	0.0
	Average B-Factors (Å <sup>2</sup> )		
protein	37.5	55.6	52.3
ligand	56.2	67.3	58.1
water	42.7	35.8	42.9
	Number of Atoms		
protein	5669	5603	5625
ligand	118	109	95
water	553	39	59
PDB code	6SUK	6XVP	6SVY

<sup>a</sup>Inner shell, overall, and outer shell statistics are given in square brackets, unbracketed, and round brackets, respectively.

reduce angiotensin II levels and blood pressure, while bradykinin levels did not increase.<sup>20</sup> Other studies showed that only lisinopril and not Lis-W caused a decrease in nACE-specific substrates Ac-SDKP and Ang 1–7 levels.<sup>21,22</sup> These results show that low levels of cACE selectivity are unlikely to give the desired reduction in side effects and highlight the importance of including a good level of selectivity for cACE in the design of future vasopeptidase inhibitors.

Previously, we reported the high-resolution crystal structures of individual domains of ACE in complex with omapatrilat, sampatrilat, and samASP.<sup>9,23</sup> Omapatrilat displayed non-selective inhibition, inhibiting both nACE and cACE in the subnanomolar range, and the structural results highlighted conserved protein–inhibitor interactions for the Zn<sup>2+</sup>-bound omapatrilat molecule within the active site of each domain. Further, the complex with cACE showed that two additional omapatrilat molecules were able to bind in the binding site cavity, consistent with binding of an omapatrilat dimer. This lends support for the design of an extended molecule exploiting the larger active site groove to provide enhanced specificity for cACE. The crystal structures of sampatrilat and samASP in complex with ACE domains provided a molecular basis for differences in inhibitor affinity and selectivity for nACE and cACE.

Here, we describe the crystal structures of NEP in complex with omapatrilat, sampatrilat, and samASP. The structural data are consistent with the inhibition data and show clear protein–inhibitor interactions involving the Zn<sup>2+</sup> ion at the active site and S<sub>1</sub>' to S<sub>2</sub>' subsites in all three complexes. Our findings and analysis also provide clear differences and experimental insights into ligand binding in comparison to domain-specific ACE active site pockets that are important for the design of highly specific dual NEP/ACE inhibitors.

## RESULTS

### Overall Structure of Inhibitor–NEP Complexes.

Crystals of NEP extracellular domain (residues 51Y–749W) in complex with omapatrilat, sampatrilat, and samASP (Table 1) were grown by either co-crystallization or soaking. The crystals of all three complexes belonged to the P3<sub>2</sub>21 space group and contained one molecule of the protein in the asymmetric unit. The structures were solved by molecular replacement using the substrate-free NEP structure PDB code 6GID with resolutions of 1.75, 2.65, and 2.6 Å for NEP–omapatrilat, NEP–sampatrilat, and NEP–samASP complexes, respectively (Table 2).

The overall structure of all three complexes shows the typical, mainly  $\alpha$ -helical ellipsoid shape previously observed for NEP, which is composed of subdomain 1 (mostly N-domain residues), a linker region, and subdomain 2 (mostly C-terminal residues) (Figure 1). All of the structures show N-linked glycosylation of asparagines 144, 284, and 324 from subdomain 2 and 627 from subdomain 1, with a single N-acetylglucosamine residue observed at each site (Figure 1).

The subdomains and linker region form a large central cavity, which contains the catalytic site that is located within subdomain 1 (Figure 1). This catalytic site comprises a zinc ion, a zinc-binding residue Glu-646, and the conserved zinc metalloprotease motif <sup>583</sup>HEXXH<sup>587</sup> (His-583 and His-587 complete the zinc binding, while Glu-584 is a catalytic residue). Examination of the mFo–DFc omit and final 2mFo–DFc maps adjacent to the zinc ion of the complex structures revealed clear and unambiguous electron density for

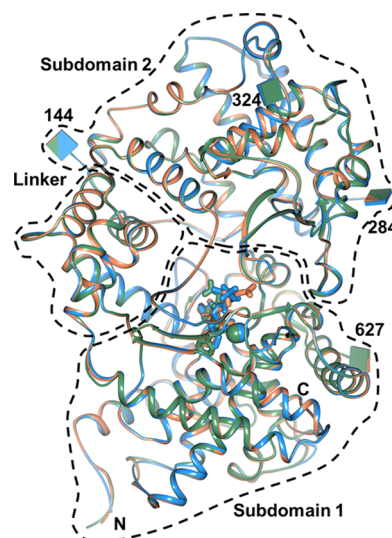


**Figure 1.** Schematic overlay representation showing the subdomain arrangement of the omapatrilat–NEP (PDB ID: 6SUK), sampatrilat–NEP (PDB ID: 6XVP), and samASP–NEP (PDB ID: 6SVY) complex structures colored in green, blue, and orange, respectively. Active site zinc ions are depicted as spheres, inhibitor molecules as sticks, and the glycosylation sites as glycoblocks (labeled with the corresponding asparagine residue number). Loop regions have been shortened for clarity.

the bound inhibitors (Figure 2), the details of which are described below.

**Omapatrilat Binding Site.** The omapatrilat molecule interacts with NEP along its entire length (Figures 3A and 4A); a full list of these interactions is shown in Table 3. Omapatrilat was designed as a tripeptide mimic with the aim of binding to the S<sub>1</sub>, S<sub>1</sub>', and S<sub>2</sub>' subsites of the target metalloproteases. However, in the NEP complex structure, it is largely bound in the S<sub>1</sub>' and S<sub>2</sub>' subsites, with part of the bicyclic group extending toward the S<sub>3</sub>' region (Figure 5).

The thiol group of omapatrilat coordinates to the zinc ion as well as two water molecules that mediate interactions with His-711 and the backbone of Ala-543. The phenyl group of omapatrilat extends deep inside the S<sub>1</sub>' pocket, where it forms extensive hydrophobic interactions with Phe-106, Phe-563, Val-580, and Trp-693, as well as a further hydrophobic interaction from its C $\alpha$  equivalent atom with His-583. The P<sub>1</sub>' carbonyl group of omapatrilat has a hydrophobic interaction from C11 to His-711 and a bidentate interaction from O4 with Arg-717. Both N2 and O3 of the omapatrilat P<sub>2</sub>' peptide bond mimic interact with Asn-542, while C2 has a hydrophobic interaction with His-711. The seven-membered fused ring only partially extends into the S<sub>2</sub>' pocket, but still makes hydrophobic interactions with Phe-106 and Trp-693. The six-membered fused ring of omapatrilat bridges toward the S<sub>3</sub>' region, and while it does not strongly interact with NEP, the backbone mimic has a hydrophobic interaction from C9 to His-711, and the “C-terminal” carboxylate group has a bidentate interaction with Arg-110.

**Sampatrilat Binding Site.** Sampatrilat binds to NEP in the S<sub>2</sub>' and S<sub>1</sub>' subsites, and unlike omapatrilat, extends past the zinc ion into the S<sub>1</sub>/S<sub>2</sub> region (Figure 5). The electron densities for the lysine-like moiety and the methanesulfonamide group in the nonprime subsites show that this region is flexible with multiple conformations likely (Figure 2B). However, there is sufficient clarity to assign which area of



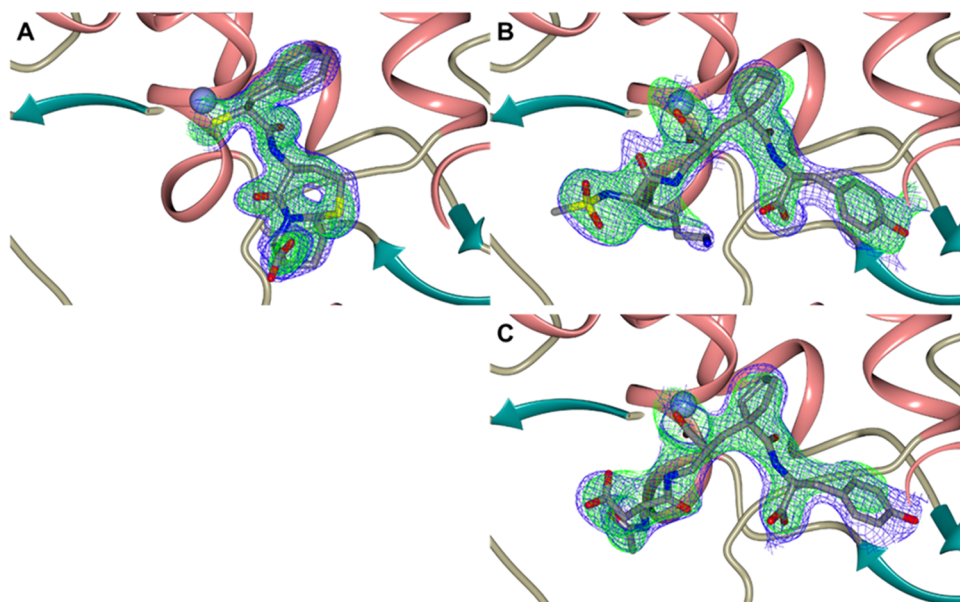


**Figure 2.** Schematic representation of inhibitors bound to NEP overlaid with the final 2mFo–DFc (blue, contoured at 1 $\sigma$  level) electron density map and the mFo–DFc (green, contoured at 3 $\sigma$  level) electron density omit map for (A) omapatrilat–NEP (PDB ID: 6SUK), (B) sampatrilat–NEP (PDB ID: 6XVP), and (C) samASP–NEP (PDB ID: 6SVY) complexes. The zinc ion is shown as a lilac sphere with the inhibitors shown as sticks.  $\alpha$ -Helices and  $\beta$ -strands are shown in rose and dark cyan, respectively.

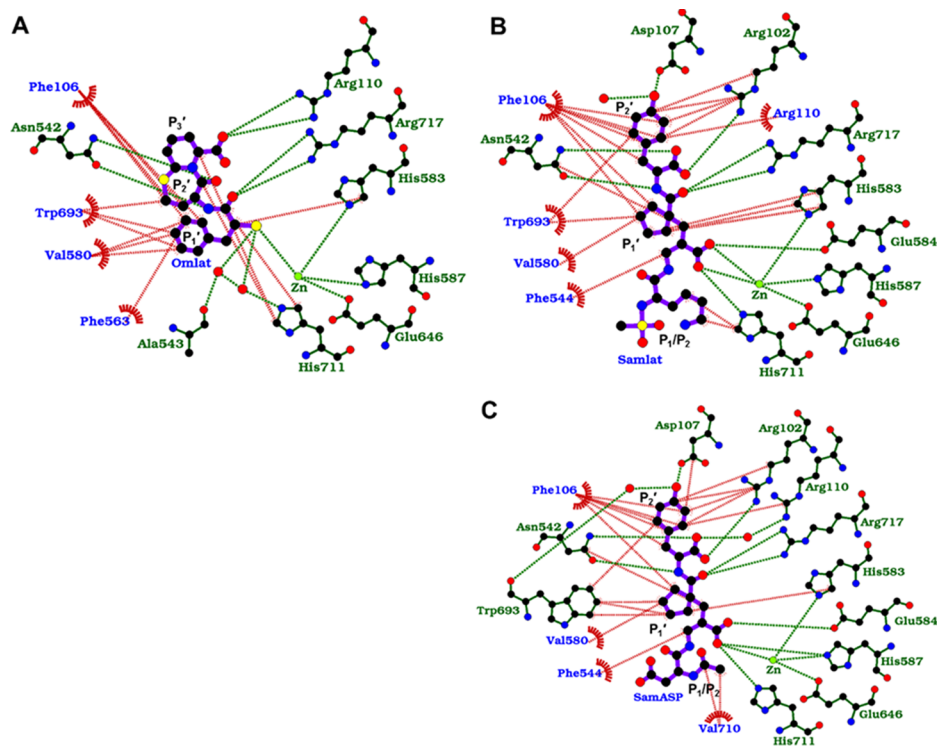


**Figure 3.** LigPlot representation of the binding site interactions of (A) omapatrilat–NEP (PDB ID: 6SUK), (B) sampatrilat–NEP (PDB ID: 6XVP), and (C) samASP–NEP (PDB ID: 6SVY) complexes. Hydrogen-bond/electrostatic interactions are shown in green, hydrophobic interactions in red, and water molecules as red spheres. Residues solely involved in hydrophobic interactions are represented by red, semicircular symbols. The inhibitor moieties are given their “P” number based on the enzyme S-subsite to which they bind.

electron density corresponds to the methanesulfonamide group due to the strong signal from the sulfur atom being still visible beyond 3 $\sigma$  in the 2mFo–DFc map. All interactions are listed in Table 3 and shown in Figures 3B and 4B. The only interactions with NEP for these groups of sampatrilat are two hydrophobic interactions between the lysine-like moiety and His-711, and

this is consistent with the flexibility indicated by the electron density.

There are considerably more interactions shown in the zinc-binding region, as well as S<sub>1</sub>' and S<sub>2</sub>' subsites. The zinc-binding region has hydrophobic interactions from “backbone” P<sub>1</sub> C15 and P<sub>1</sub>' C17 of sampatrilat with Phe-544 and Asn-542,



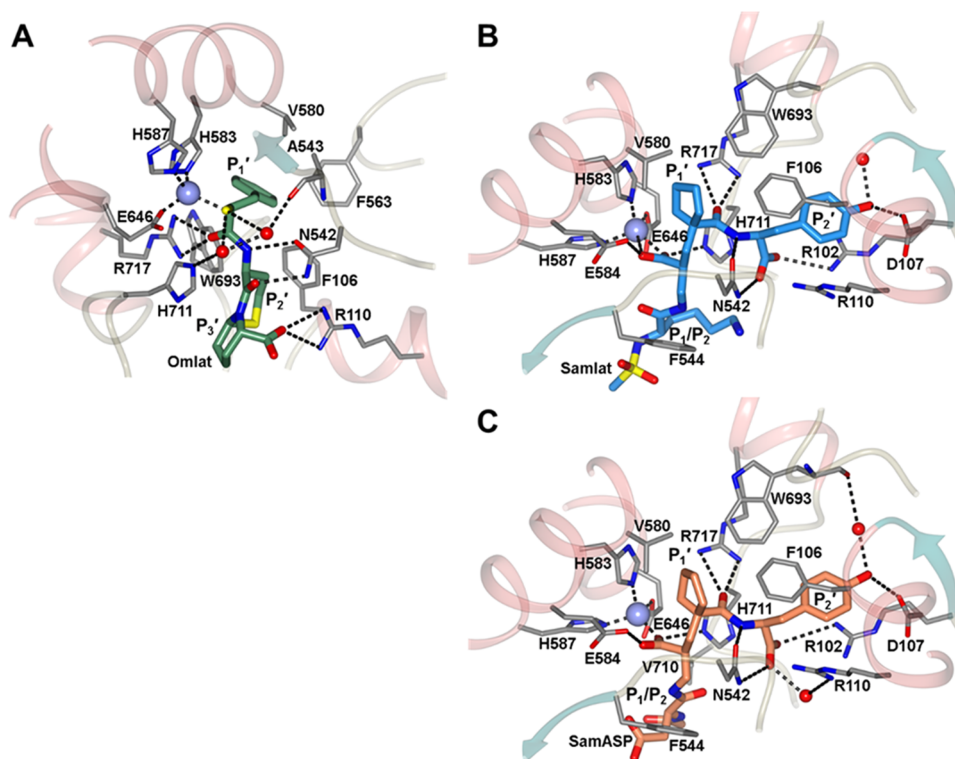


**Figure 4.** Close-up views of (A) omapatrilat–NEP (PDB ID: 6SUK), (B) sampatrilat–NEP (PDB ID: 6XVP), and (C) samASP–NEP (PDB ID: 6XVY) binding sites showing hydrogen-bond/electrostatic interactions (dashed lines). The inhibitor molecules are depicted as fat sticks, protein chain as a cartoon with  $\alpha$ -helices and  $\beta$ -strands in rose and dark cyan, respectively, zinc ion as lilac sphere, and water molecules as red spheres. The inhibitor moieties are given their P number based on the enzyme S-subsite to which they bind.

**Table 3. Comparison of Amino Acid Residues Involved in Omapatrilat, Sampatrilat, and SamASP Binding to NEP<sup>a</sup>**

subsite	omapatrilat			sampatrilat			samASP		
	DHB	WIM	HPB	DHB	WIM	HPB	DHB	WIM	HPB
S <sub>3</sub> '	Arg110		His711						
S <sub>2</sub> '			Phe106	Arg102		Arg102	Arg102	Arg110	Arg102
	Asn542			Asp107		Phe106	Asp107	Trp693	Phe106
				Asn542			Asn542		Asp107
			Trp693			Arg110			Arg110
			His711						Trp693
S <sub>1</sub> '	Arg717		Phe106	Arg717		Phe106	Arg717		Phe106
			Phe563			Asn542			Asn542
			Val580			Val580			Val580
			His583			His583			His583
			Trp693			Trp693			Trp693
Zn-binding atoms		Ala543							
		His583			His583			His583	
		His587			His587			His587	
		Glu646			Glu646			Glu646	
		His711							
S <sub>1</sub>				Glu584		Phe544	Glu584		Phe544
				His711			His711		
S <sub>2</sub>						His711			Val710

<sup>a</sup>DHB—direct hydrogen-bond interactions, WIM—water/ion-mediated interactions, HPB—hydrophobic interactions.

respectively. In addition, the P<sub>1</sub> C16 carboxy group is strongly coordinated via a bidentate interaction with the zinc ion and hydrogen-bonds with Glu-584 and His-711. The P<sub>1</sub>' ring of sampatrilat extends into the S<sub>1</sub>' subsite, where it has extensive hydrophobic interactions with Phe-106, Val-580, His-583, and

Trp-693. The backbone P<sub>1</sub>' carbonyl and P<sub>2</sub>' nitrogen have interactions with Arg-717 (bidentate) and Asn-542, respectively. The P<sub>2</sub>' tyrosine side chain of sampatrilat extends deep into the S<sub>2</sub>' pocket, where it forms stacking hydrophobic interactions between the ring of Phe-106 and side chain of Arg-

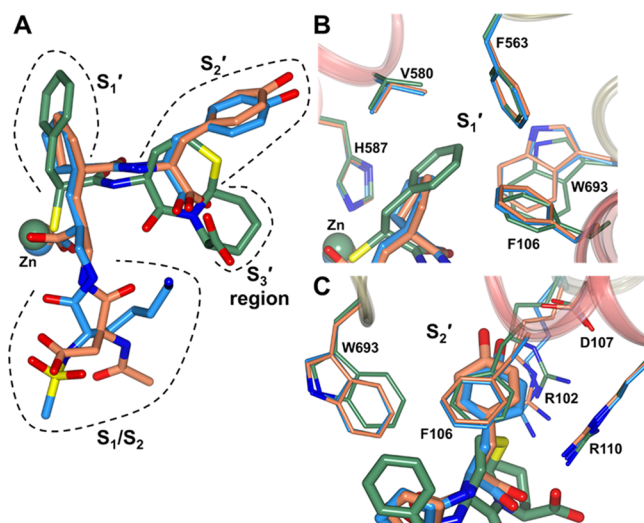


**Figure 5.** Comparison of omapatrilat–NEP (PDB ID: 6SUK), sampatrilat–NEP (PDB ID: 6XVP), and samASP–NEP (PDB ID: 6SVY) binding sites colored green, blue, and orange, respectively. Inhibitors are depicted as sticks and zinc ions as spheres. (A) Overlay of inhibitors from the crystal structures with the subsite binding pockets indicated. (B) Close-up overlay view of the  $S_1'$  pocket. (C) Close-up overlay view of the  $S_2'$  pocket.

102, as well as a further hydrophobic interaction with Arg-110. In addition, the  $P_2'$  O34 atom forms hydrogen bonds with Asp-107 and a water molecule. Finally, the  $P_2'$  carboxy terminus of sampatrilat has two hydrogen bonds with Arg-102 and Asn-542.

**SamASP Binding Site.** SamASP binds to NEP in a similar orientation to sampatrilat occupying the  $S_2'$  and  $S_1'$  subsites, zinc-binding region, and extending into the nonprime subsites (Figure 5). In the nonprime region, the secondary amide and aspartate side-chain-like groups on C5 of samASP are of equivalent size. The electron density observed in the maps is not clear enough to unambiguously assign which group should be placed in which patch of density (Figure 2C). The best-fit model had the aspartate-like carboxy group placed in the strongest patch of density, with the secondary amide positioned such that its C1 and C2 atoms formed hydrophobic interactions with Val-710 (Figures 3C and 4C). These are the only interactions observed with this section of samASP, along with the ambiguous electron density that is consistent with probable multiple conformations of these groups. All interactions are listed in Table 3.

The  $P_1$  zinc-binding carboxy group of samASP has a single interaction with the zinc ion as well as two hydrogen bonds with Glu-584 and His-711. The backbone  $P_1$  C13 and  $P_1'$  C15 atoms on either side of this carboxy group form hydrophobic interactions with Phe-544 and Asn-542, respectively. The  $S_1'$  subsite residues Phe-106, Val-580, His-583, and Trp-693 form extensive hydrophobic interactions with the  $P_1'$  cyclopentyl group of samASP, while the  $P_1'$  backbone carbonyl has a bidentate interaction with Arg-717. Asn-542 forms hydrogen bonds with the  $P_2'$  backbone nitrogen and carboxy terminus. This carboxy terminus also interacts with Arg-102 and has a water-mediated hydrogen bond with Arg-110. The  $P_2'$  tyrosine-like side chain forms extensive hydrophobic interactions deep in the  $S_2'$  pocket with Asp-107, Arg-110, Trp-693, and stacking between Phe-106 and Arg-102. The O32 atom of

this  $P_2'$  side chain has hydrogen bonds with Asp-107 and Trp-693 (water-mediated).

## DISCUSSION

**Comparison of Omapatrilat–NEP, Sampatrilat–NEP, and SamASP–NEP Structures.** An overlay of the three inhibitor–NEP complexes presented here (Figure 1) show that the binding of these inhibitors has very little effect on the overall structure, and this is reflected by the root-mean-square deviation (RMSD) values for the 696  $C\alpha$  atoms observed in all structures being 0.27 Å at most (Table 4). Comparison of the

**Table 4. Comparison of the Overall Inhibitor–NEP Complex Structures<sup>a</sup>**

	sampatrilat	samASP	native (PDB ID: 6GID)
omapatrilat	0.272	0.230	0.334
sampatrilat		0.196	0.370
samASP			0.356

<sup>a</sup>RMSD values (Å) for 696  $C\alpha$  atoms observed in all structures. Values were generated using the “Structure Alignment and Superposition with Gesamt” program on CCP4 cloud.

inhibitor–NEP structures with a previous NEP structure with no ligand added (PDB code: 6GID) shows again very little difference in the structure with RMSD values of the 696  $C\alpha$  atoms all less than 0.37 Å. While this shows that ligand-bound structures are more similar to each other than to native NEP, it is a very small difference, and essentially the structures remain the same.

An overlay of sampatrilat and samASP inhibitors from the NEP complex structures (Figure 5) shows that the zinc-binding region and  $P_1'$  and  $P_2'$  groups largely bind to NEP in the same position and orientation. There are some small differences in these regions, for example, orientation of the zinc-binding carboxylate and  $P_2'$  tyrosine side chain, but these all result in changes of less than 1 Å, and nearly all of the interactions are conserved for this part of the inhibitors (Figure 3B,C). This is not surprising as the zinc-binding region and  $P_1'$  and  $P_2'$  groups are identical between sampatrilat and samASP. In contrast, this overlay shows that the nonprime parts of sampatrilat and samASP, while occupying a similar spatial location in NEP, have significant differences in orientation. This even applies to backbone nitrogen and carbonyl that are immediately adjacent to the zinc-binding region and conserved between sampatrilat and samASP. These atoms are flipped 180° compared to each other (Figure 4B,C), although it is unclear from the crystal structures what causes this change considering there are no strong interactions between these atoms and NEP. Instead, this may be driven by the ligand chemical composition itself with the differences in the  $P_2$  groups causing the flip. It is likely that this flip causes the small orientation change of the zinc-binding carboxylate and, subsequently, the  $P_1'$  and  $P_2'$  groups described above. These ligands only differ in their  $P_2$  groups, but these groups still largely occupy similar regions of the nonprime NEP binding site, although the lysine-like moiety of sampatrilat does not overlay well with the carbonyl group of samASP (Figure 5A). However, the electron density indicates that the  $P_2$  groups of both ligands are flexible, in particular the lysine-like side chain of sampatrilat, and this is likely due to the lack of interactions with NEP.

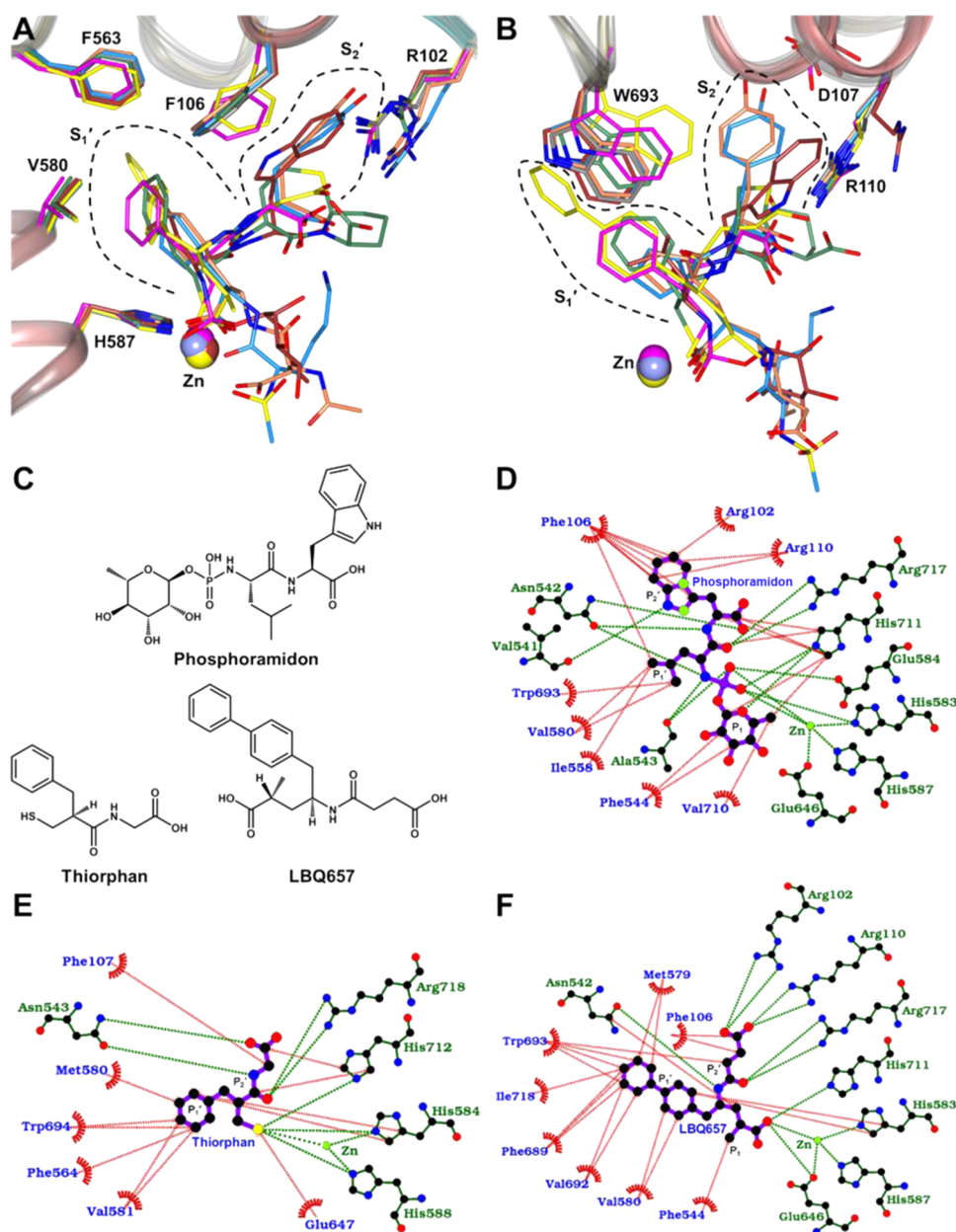


**Figure 6.** Comparison of omapatrilat–NEP (PDB ID: 6SUK), sampatrilat–NEP (PDB ID: 6SVP), and samASP–NEP (PDB ID: 6SVY) binding sites with native NEP and previous inhibitor–NEP complex structures. Structures of native NEP, LBQ657–NEP, thiorphan–NEP, and phosphoramidon–NEP used PDB codes 6GID, 5JMY, 5V48, and 1DMT, respectively. (A, B) Two views of the  $S_1'$  and  $S_2'$  subsites with residues from these subsites involved in interacting with the ligands shown in only one of the views for clarity. Omapatrilat–NEP, sampatrilat–NEP, samASP–NEP, native NEP, phosphoramidon–NEP, thiorphan–NEP, and LBQ657–NEP are shown in green, blue, orange, gray, brown, magenta, and yellow, respectively. (C) Chemical structures of phosphoramidon, thiorphan, and LBQ657. (D–F) LigPlot representation of the binding site interactions of phosphoramidon–NEP, thiorphan–NEP, and LBQ657–NEP complexes. Hydrogen-bond/electrostatic interactions are shown in green, hydrophobic interactions in red, and water molecules as red spheres. Residues solely involved in hydrophobic interactions are represented by red, semicircular symbols. The inhibitor moieties are given their P number based on the enzyme S-subsite to which they bind. Note that the structure of thiorphan is in complex with rabbit NEP with residues having a slightly different numbering.

The overlay of omapatrilat with sampatrilat and samASP (Figure 5A) shows that omapatrilat occupies a similar space in the prime subsites as the other inhibitors, but as mentioned previously, unlike sampatrilat and samASP, omapatrilat does not extend into the nonprime side of the zinc-binding site. This is because the phenyl group of omapatrilat binds in the  $S_1'$  pocket of NEP, and as this phenyl group is longer than the  $P_1'$  ring of sampatrilat and samASP, it extends further into the  $S_1'$  pocket and is involved in more hydrophobic interactions (Figures 3 and 5B). In contrast, the bicyclic ring of omapatrilat

is too bulky to enter very far into the  $S_2'$  pocket, but just binds at the entrance. However, the tyrosine-like side chain of sampatrilat and samASP extends deep into the  $S_2'$  pocket resulting in many more binding interactions than omapatrilat, including the hydrogen bond with Asp-107 and the strong stacking interactions with Phe-106 and Arg-102 (Figures 3 and 5C). While omapatrilat does extend further toward the  $S_3'$  subsite than sampatrilat or samASP, because of the binding orientation, its C-terminal mimic carboxylate group is located close to the equivalent carboxylate group of sampatrilat and



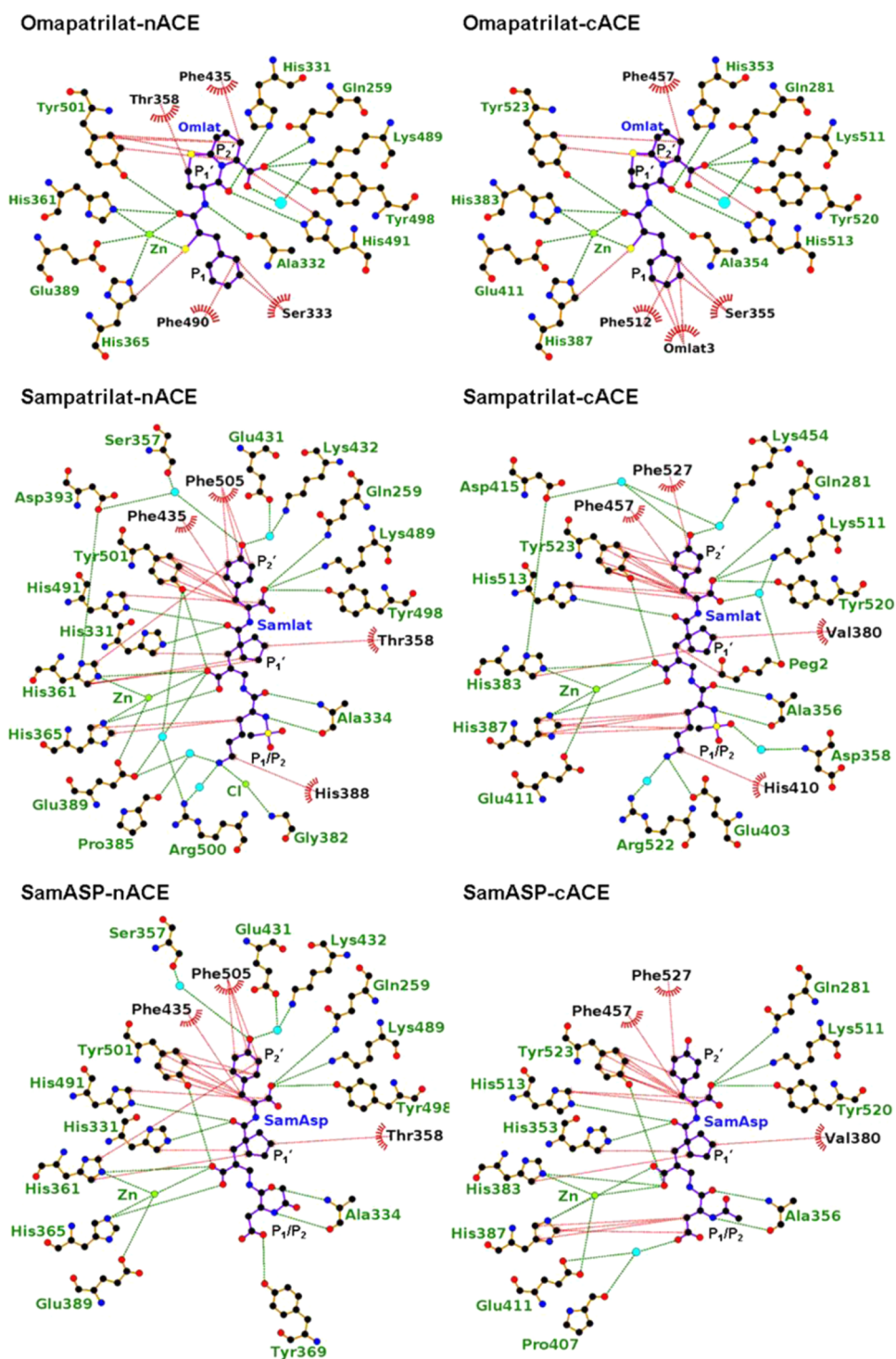


**Figure 7.** LigPlot representation of the binding site interactions of omapatrilat–nACE (PDB ID: 6H5X), omapatrilat–cACE (PDB ID: 6H5W), sampatrilat–nACE (PDB ID: 6F9V), sampatrilat–cACE (PDB ID: 6F9T), samASP–nACE (PDB ID: 6F9R), and samASP–cACE (PDB ID: 6F9U) complexes. Hydrogen-bond/electrostatic interactions are shown in green, hydrophobic interactions in red, and water molecules as red spheres. Residues solely involved in hydrophobic interactions are represented by red, semicircular symbols. The inhibitor moieties are given their P number based on the enzyme S-subsite to which they bind.

samASP, but directly interacts with different NEP residues (Figures 3 and 5A). While overall omapatrilat shows less interactions with NEP than sampatrilat and samASP do, these interactions are spread over the whole molecule, unlike sampatrilat and samASP, which have a significant portion of their structure being weakly bound in the nonprime region of

NEP, and this is consistent with omapatrilat and sampatrilat both having high potency for NEP (Table 1).

**NEP Binding Comparison of Omapatrilat, Sampatrilat, and SamASP with Other Inhibitor–NEP Complexes.** NEP has been previously crystallized in complex with phosphoramidon (PDB codes human: 1DMT and rabbit: 4ZR5),<sup>24,25</sup> thiorphan (PDB code: 5V48),<sup>24</sup> and LBQ657

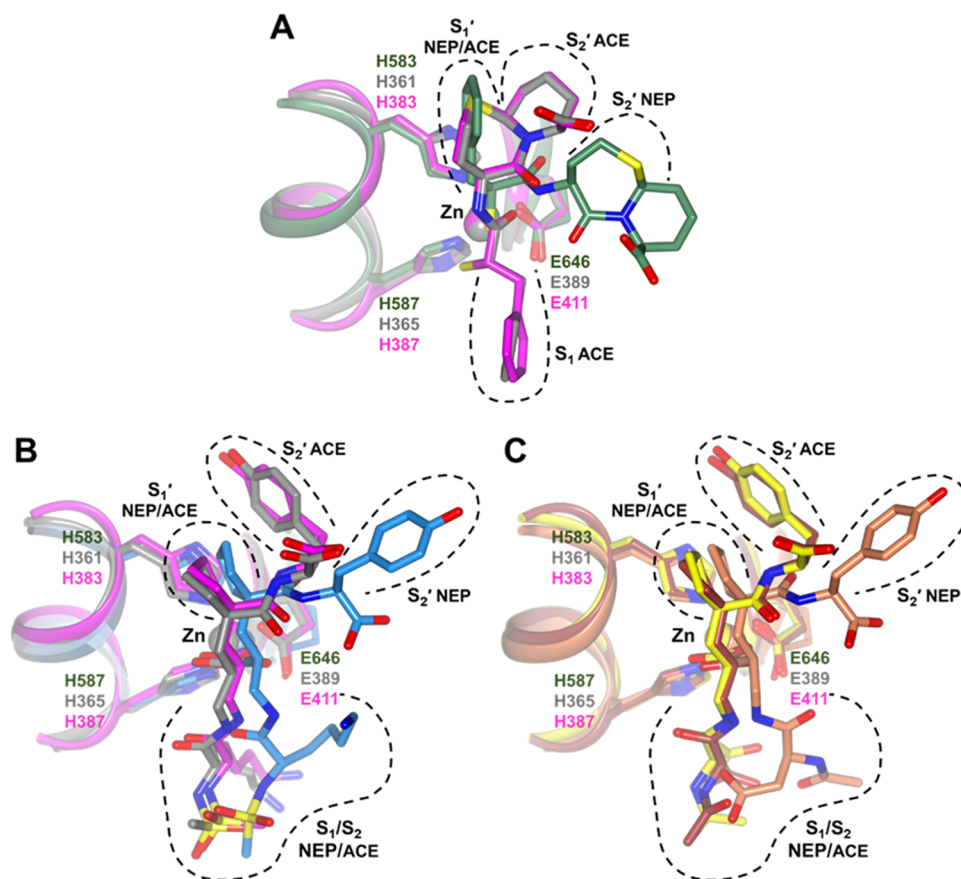


**Figure 8.** Comparison of inhibitor binding sites between NEP and ACE domains. The zinc ion and its binding residues were used to overlay the structures. (A) Omapatrilat binding site with NEP (PDB ID: 6SUK), nACE (PDB ID: 6HSX), and cACE (PDB ID: 6HSW) structures shown in green, magenta, and gray, respectively. NEP, nACE, and cACE binding sites for (B) sampatrilat (blue PDB ID: 6XVP, magenta PDB ID: 6F9V, and gray PDB ID: 6F9T) and (C) samASP (orange PDB ID: 6SVY, brown PDB ID: 6F9R, and yellow PDB ID: 6F9U). The subsite pockets for NEP and ACE domains are indicated.

(PDB code: 5JMY)<sup>26</sup> (chemical structures of these ligands are shown in Figure 6C). Thiorphan and LBQ657 are the active forms of the prodrugs racemadotril and sucubitril, respectively. A recent study using purified enzymes showed that both thiorphan and LBQ657 were equally potent NEP inhibitors (IC<sub>50</sub> values of 20 nM for both) and were highly specific compared to the weak inhibition of ACE (10.2 and >100 μM, respectively).<sup>27</sup> Furthermore, a previous study using partially purified enzymes showed that phosphoramidon was also a potent and specific inhibitor for NEP over ACE (IC<sub>50</sub> values of 34 nM and 78 μM, respectively).<sup>28</sup> As described previously, both omapatrilat and sampatrilat are also potent inhibitors of NEP (IC<sub>50</sub> value of 8 nM for both).<sup>10,14</sup> While IC<sub>50</sub> values from different assays and different research groups cannot be directly compared, it is clear that all of these compounds are potent NEP inhibitors, so a comparison of their structures can indicate what modes of binding are able to produce this potent inhibition.

An overlay of the inhibitors from these NEP complex structures (Figure 6) shows that sampatrilat, samASP, and phosphoramidon have groups that extend deep into the S<sub>1</sub>/S<sub>2</sub> subsite region, with only phosphoramidon having a significant number of interactions with NEP (LigPlot+ diagrams showing the interactions of phosphoramidon, thiorphan, and LBQ657 are shown in Figure 6D–F, respectively). These include hydrophobic interactions with Phe-544, Val-710, and His-711, as well as a hydrogen bond with His-711. LBQ657 has a short

methyl P<sub>1</sub> group that only interacts with Phe-544 of NEP, whereas both omapatrilat and thiorphan lack P<sub>1</sub> groups, and therefore terminate with the zinc-ion interactions. This is consistent with previous observations that P<sub>1</sub> groups at best only give a small increase in affinity.<sup>29–31</sup> The other end of the inhibitor molecule can target residues that would bind the P<sub>2</sub>' backbone carbonyl or C-terminal carboxy group of NEP peptide substrates, and these residues include Arg-102, Arg-110, and Asn-542. All of the inhibitors compared here contain a carboxy group that interacts with one or more of these residues, even omapatrilat which extends a little further into the prime subsites than the other inhibitors.

In contrast to the P<sub>1</sub> position, groups at P<sub>1</sub>' and P<sub>2</sub>' are crucial in providing multiple interactions with NEP to produce potent inhibitors. The S<sub>1</sub>' pocket is hydrophobic; formed by residues Phe-106, Ile-558, Phe-563, Met-579, Val-580, Phe-689, Val-692, Trp-693, and Ile-718; and preferentially binds to large hydrophobic or aromatic P<sub>1</sub>' groups.<sup>32</sup> Phe-106 and Trp-693 separate the S<sub>1</sub>' and S<sub>2</sub>' pockets, thereby giving a hydrophobic face to the large S<sub>2</sub>' subsite. Residues Arg-102, Asp-107, Arg-110, and Val-541 form the rest of the S<sub>2</sub>' pocket, and therefore this subsite is less specific and can bind to a range of moieties to increase affinity. The inhibitors compared here provide a range of examples and different ways to maximize interactions and therefore increase affinity for NEP within the S<sub>1</sub>' and S<sub>2</sub>' subsites (Figure 6A,B). First, all of the inhibitors contain a P<sub>1</sub>' carbonyl and P<sub>2</sub>' nitrogen peptide

backbone mimic, which interact with Arg-717 and Asn-542, respectively. Sampatrilat, samASP, and phosphoramidon contain fairly short  $P_1'$  groups that only extend partway into the  $S_1'$  pocket. Therefore, they have less hydrophobic interactions with NEP than omapatrilat and thiorphan do, which have more bulky phenyl groups that extend further into the pocket. LBQ657 has the longest  $P_1'$  group, a biphenyl, which extends deep into the pocket and can interact with most of the hydrophobic pocket. As mentioned above, Phe-106 and Trp-693 divide the  $S_1'$  and  $S_2'$  pockets, and it has been previously reported that a  $P_1'$  biphenyl causes a conformational change in the side chains of these residues. It is interesting to note that when comparing all of the structures here, this conformational change is also observed with smaller  $P_1'$  side chains, and the degree of movement correlates with the size of the  $P_1'$  group. Among these inhibitors, the  $P_2'$  side chain varies from nothing (LBQ657 and thiorphan), extending partially into the  $S_2'$  pocket (omapatrilat) and deep into the pocket (sapatrilat, samASP, and phosphoramidon). Therefore, the inhibitors with the most interactions in the  $S_1'$  pocket (LBQ657, thiorphan, and omapatrilat) have the least in the  $S_2'$  pocket. The phenyl side chains of sapatrilat and samASP occupy a different position in the  $S_2'$  pocket than the indole side chain of phosphoramidon and therefore have different interactions with NEP. All three cause a change in the orientation of Arg-102, as does omapatrilat to a lesser extent. In addition, there is a large shift in the side chain of Arg-110 in the phosphoramidon–NEP structure. These side-chain orientation changes show that both the  $S_1'$  and  $S_2'$  pockets can adapt to the size and shape of the  $P_1'$  and  $P_2'$  groups, but further screens are needed to examine how the size of one  $P'$  group effects the possible size of the other.

**Comparison of Omapatrilat, Sapatrilat, and SamASP Binding to NEP and ACE Domains.** Crystal structures of both domains of sACE have been solved in complex with omapatrilat (PDB codes: 6HSX for nACE and 6HSW for cACE),<sup>9</sup> sapatrilat (PDB codes: 6F9V for nACE and 6F9T for cACE), and samASP (PDB codes: 6F9R for nACE and 6F9U for cACE),<sup>23</sup> and this allows direct comparison of inhibitor binding with the NEP structures presented here (LigPlot+ diagrams showing the interactions of omapatrilat, sapatrilat, and samASP with nACE and cACE are shown in Figure 7).

When the active site zinc and its binding residues are used as the basis to orientate and compare structures of NEP and the ACE domains, the  $S_1'$  and  $S_1/S_2$  subsites essentially overlay and occupy the same space (Figure 8). All of the inhibitors bind to the ACE domains in a close-to-linear backbone conformation consistent with there being distinctive prime and nonprime lobes on either side of the zinc ion. In contrast, NEP contains a single large cavity that causes ligands to bind in a conformation that is bent between the  $S_1'$  and  $S_2'$  subsites. This has the effect that in the NEP and ACE domain comparison, the  $S_2'$  binding pockets do not overlay (Figure 8).

In both ACE domains, omapatrilat binds with the phenyl ring extending into the  $S_1$  subsite and the bicyclic moiety located in the  $S_1'$  and  $S_2'$  pockets (Figure 8A). However, the requirement for ligands to adopt a bent conformation when binding to NEP in the  $S_1$ ,  $S_1'$ , and  $S_2'$  subsites is likely to be the cause of omapatrilat binding in a different manner, not utilizing the  $S_1$  subsite and instead having the phenyl and bicyclic groups in the  $S_1'$  and  $S_2'/S_3'$  pockets, respectively. In contrast, sapatrilat and samASP bind in a similar manner to both NEP

and the ACE domains, where the tyrosine-like side-chain and cyclopentane ring occupy the  $S_2'$  and  $S_1'$  pockets, respectively, and the remainder of the molecules binds to the  $S_1$  and  $S_2$  subsites (Figure 8B,C).

A comparison of interactions between inhibitor and protein for the NEP and ACE domain structures (Figures 3 and 7) provides detailed information on what to target for potency and specificity. With ACE being predominantly a dipeptidase, there are strong interactions possible at the C-terminal carboxy  $P_2'$  position, as well as with carbonyl or nitrogen peptide backbone mimics in both the  $S_1'$  and  $S_2'$  subsites. All three inhibitors studied here utilize all of these interactions with both domains of ACE. Although not quite as extensive in NEP, interactions with ligand backbone atoms are still important for a high affinity inhibitor.

In structures of both enzymes, omapatrilat, sapatrilat, and samASP all have hydrophobic interactions in the  $S_2'$  pocket, and a greater number of interactions are observed when the  $P_2'$  group is larger. This is highlighted by comparing the tyrosine-like group of sapatrilat and samASP that extends further into the  $S_2'$  subsite, with the less elongated bicyclic ring of omapatrilat. The hydroxyl group of this tyrosine also shows that direct and water-mediated interactions are possible in this pocket in both NEP and the ACE domains.

All three inhibitors have some hydrophobic interactions in the  $S_1'$  pocket of the ACE domains, and this is likely to be stronger in cACE due to Val-380 being replaced by Thr-358 in nACE. In comparison, there is a much more extensive network of hydrophobic interactions in the NEP  $S_1'$  pocket, and this is especially apparent with the large  $P_1'$  phenyl group of omapatrilat.

NEP and both ACE domains have more space available in the nonprime binding sites than the prime sites. In NEP, this has the effect of very few interactions observed with the  $P_1/P_2$  sections of sapatrilat and samASP, and this causes the more ambiguous electron density for this region described above. In contrast, although there is extra space available in the ACE domain nonprime lobe, there are still many residues in the  $S_1/S_2$  subsites available to target for both hydrophobic interactions as seen with the phenyl group of omapatrilat, and a range of electrostatic and hydrogen bonds (direct and water-mediated) as observed with sapatrilat and samASP.

In summary, the structures of the complexes with these three inhibitors show that the ACE domains have a significant number of interactions with the backbone and side chains throughout the  $S_2$  to  $S_2'$  subsites, whereas NEP is largely reliant on its zinc-binding region and  $S_1'$  to  $S_2'$  subsites, with the added requirement that if the inhibitor extends into the nonprime subsites, then it needs to be able to adopt a bent conformation between  $P_1'$  and  $P_2'$ .

### Conclusions and Structure-Based Design Toward Next-Generation Dual cACE Selective/NEP Inhibitors.

As described above, vasopeptidase inhibitors have been designed to increase the control of blood pressure by targeting both RAAS and NPKS. While omapatrilat does this very effectively, it results in even more severe side effects than typical ACE only inhibition. This is thought to be due to the accumulation of bradykinin (and substance P), a substrate for both NEP and ACE, with omapatrilat showing potent inhibition of NEP, nACE, and cACE. It has previously been shown that blood pressure can be controlled by inhibition of cACE alone, which would leave nACE activity intact to control bradykinin levels. This approach would be beneficial for



vasopeptidase inhibitors as well as targeting only ACE; therefore, structural data presented here and from previous studies can be used to design inhibitors that are not only potent for NEP but also specific for cACE over nACE. ACE has a  $K_m$  value of 0.18  $\mu\text{M}$  for bradykinin,<sup>33</sup> which indicates that for an inhibitor with a desired potent low nM affinity for cACE, the specificity over nACE would need to be at least 2 orders of magnitude.

The comparison of NEP structures has shown that binding to nonprime subsites only provides a small increase in affinity, and therefore not surprisingly, potent inhibition is possible with binding to the zinc-binding region and  $S_1'$  to  $S_2'$  subsites. The  $S_1'$  and  $S_2'$  subsites provide backbone hydrogen bonding as well as extensive hydrophobic interactions within the side-chain binding pockets, where the further the side chain extends into the pocket, the greater the number of interactions. In addition, the  $S_2'$  pocket is less specific than  $S_1'$  with hydrogen-bonding targets also possible, and both pockets have flexibility in side chains to allow binding of inhibitor moieties of different sizes. It is also important to consider that a potent NEP inhibitor does not need to maximize interactions in both  $S_1'$  and  $S_2'$  binding pockets at the same time. This could be beneficial considering thiorphan, phosphoramidon, and, in particular, LBQ657 show specificity for NEP over ACE, and it is potentially the large  $P_1'$  moieties of these ligands that reduce the potency against ACE by causing steric clashes in the  $S_1'$  subsite. Therefore, NEP potency can be achieved with moderate size  $P_1'$  and larger  $P_2'$  moieties that can be accommodated by ACE.

Sampatrilat shows over a 12-fold specificity for cACE over nACE, whereas samASP is nondomain selective and less potent against both ACE domains. This highlights the importance of the nonprime binding region in the design of not only potent ACE inhibitors but also in making them domain-specific. A direct hydrogen bond between the lysine-like side chain of sampatrilat with Glu-403 of cACE, which is mutated to Arg-381 in nACE, explains the domain specificity, while the reduction in nonprime interactions with samASP is consistent with the reduced affinity. RXPA380 is another inhibitor that shows cACE specificity over nACE (3000-fold lower  $K_i$ ).<sup>34</sup> This was also partly attributed to differences in the  $S_1$  and  $S_2$  subsites between nACE and cACE. RXPA380 contains  $P_1$  and  $P_2$  phenyl rings that form extensive hydrophobic interactions with cACE, and of particular interest are those with Phe-391 and Val-518, which are replaced in nACE by the polar, neutral Tyr-369 and Thr-496, respectively. In addition, RXPA380 has a  $P_2'$  tryptophan group, and this has also been found to add cACE specificity. As mentioned above, including a larger  $P_2'$  group would also be a way of increasing NEP potency. Finally a study on a series of phosphinic inhibitors showed that the stereochemistry of the  $P_1'$  position had a dramatic effect on the affinity for NEP, but not for cACE or endothelin-converting enzyme-1 (ECE-1).<sup>35</sup> This is likely caused by the nonlinear arrangement of the zinc ion and well-defined, deep  $S_1'$  and  $S_2'$  pockets of NEP described above.

In conclusion, combining the requirements of potent NEP and ACE inhibition with those for cACE selectivity allows for the design of a potent vasopeptidase inhibitor with reduced side effects compared to omapatrilat and classical ACE-targeted hypertension treatments. In principle, modification of the already NEP and ACE potent sampatrilat to increase the cACE specificity would be one approach. Combining the current lysine-like side chain, thereby retaining the interaction

with the cACE-specific Glu-403, with a bulky hydrophobic moiety like phenyl in the nonprime binding sites would allow interactions with the unique cACE Phe-391 and Val-518 residues. This modification should be tolerated by NEP due to the space available in the nonprime binding region. In addition, changing the  $P_2'$  phenyl group of sampatrilat to a tryptophan group should further enhance the cACE specificity over nACE. This  $S_2'$  pocket binding moiety is already shown to bind strongly to NEP by the inhibitor phosphoramidon. In summary, next generation vasopeptidase inhibitors could use zinc-binding  $P_1'$  and  $P_2'$  groups to give potency against NEP and ACE, and then  $P_2'$ ,  $P_1$ , and  $P_2$  moieties to not only increase potency to ACE but also crucially to provide cACE specificity over nACE.

## ■ EXPERIMENTAL SECTION

**NEP Expression and Purification.** Recombinant His-tagged human NEP (extracellular domain residues 51-742) was expressed as a secreted protein in *Pichia pastoris* GS115 and purified using Ni-NTA affinity and size exclusion chromatography, as previously described.<sup>36</sup> Briefly, the cells were incubated at 30 °C for 24 h in a buffered glycerol–complex medium before being transferred into buffered methanol–complex medium. The culture was incubated for a further 72 h at 30 °C with 100% methanol being added at 24 and 48 h to maintain the methanol concentration.

After expression, the supernatant was harvested followed by the addition of Trizma and NaCl to give final concentrations of 25 and 150 mM, respectively. A 5 mL HisTrap affinity column (GE Healthcare Bio-Sciences, Pittsburgh, PA) was used to purify NEP from the clarified supernatant using binding buffer (25 mM Trizma, 150 mM NaCl, and 2 mM  $\text{MgCl}_2$ , pH 7.5) supplemented with 250 mM imidazole for elution. A further size exclusion step (16/60 Superdex HiLoad 200 column) using the same binding buffer completed the purification, followed by concentration to 12 mg/mL. Purity was assessed using sodium dodecyl sulfate–polyacrylamide gel electrophoresis (SDS-PAGE) to be >95%.

**Ligand Preparation.** Omapatrilat was obtained from Sigma-Aldrich, while sampatrilat and samASP were synthesized as previously described.<sup>15</sup> The omapatrilat stock solution (50 mM in dimethyl sulfoxide (DMSO)) was diluted to 10 mM with NEP binding buffer. Sampatrilat and samASP stock solutions (20 mM in water) were diluted to 10 mM with NEP crystallization buffer (0.2 M  $\text{NH}_4\text{Cl}$ , 22% (w/v) PEG 3350).

**X-ray Crystallographic Studies.** The omapatrilat–NEP complex was prepared using 12 mg/mL NEP and 10 mM omapatrilat at a 1:10 molar ratio with incubation on ice for 45 min prior to crystallization. The hanging-drop vapor diffusion crystallization method was used with 1  $\mu\text{L}$  of omapatrilat–NEP complex mixed with 1  $\mu\text{L}$  of reservoir solution containing (0.2 M  $\text{NH}_4\text{Cl}$ , 20–25% (w/v) PEG 3350), followed by incubation at 18 °C. A similar co-crystallization procedure did not yield any crystal for NEP in complex with sampatrilat or samASP. Instead, clusters of native NEP crystals were soaked in crystallization buffer (0.2 M  $\text{NH}_4\text{Cl}$ , 22% (w/v) PEG 3350) containing 10 mM inhibitors and incubated overnight at 18 °C. Although this process broke up the crystal clusters, fragments of smaller single crystal were suitable for X-ray diffraction. All crystals were briefly soaked in crystallization buffer supplemented with 16% glycerol for cryo-protection and then flash frozen in liquid nitrogen prior to data collection.

X-ray diffraction data for all structures were collected on station i04 at the Diamond Light Source (Didcot, U.K.), with the crystals kept at a constant temperature (100 K) using a nitrogen stream. Images were collected using PILATUS3 6M detectors (Dectris, Switzerland). Raw data images were indexed and integrated with DIALS<sup>37</sup> and then scaled using AIMLESS<sup>38</sup> from the CCP4 suite.<sup>39</sup> Initial phases were obtained by molecular replacement with PHASER<sup>40</sup> using the native NEP structure (PDB code: 6GID<sup>36</sup>) as the search model. Further refinement was initially carried out using REFMAC<sup>41</sup> and then

Phenix,<sup>42</sup> with COOT<sup>43</sup> used for rounds of manual model building. Ligand and water molecules were added based on electron density in the mFo–DFc Fourier difference map. MolProbity<sup>44</sup> was used to help validate the structures. Crystallographic data statistics are summarized in Table 2. All figures showing the crystal structures were generated using CCP4mg,<sup>45</sup> and schematic binding interactions are displayed using LigPlot+.<sup>46</sup> The coordinates of omapatrilat–NEP, sampatrilat–NEP, and samASP–NEP complexes have been deposited in PDB with accession codes 6SUK, 6XVP, and 6SVY, respectively.

## ■ ASSOCIATED CONTENT

### Supporting Information

The Supporting Information is available free of charge at <https://pubs.acs.org/doi/10.1021/acs.jmedchem.0c00441>.

Molecular formula strings (CSV)

### Accession Codes

The atomic coordinates and structure factors for omapatrilat–NEP, sampatrilat–NEP, and samASP–NEP complexes have been deposited in the RCSB Protein Data Bank with codes 6SUK, 6XVP, and 6SVY, respectively. The authors will release the atomic coordinates and experimental data upon article publication.

## ■ AUTHOR INFORMATION

### Corresponding Author

K. Ravi Acharya – Department of Biology and Biochemistry, University of Bath, Bath BA2 7AY, United Kingdom;

orcid.org/0000-0002-3009-4058; Phone: (+44) 1225-386238; Email: [bsskra@bath.ac.uk](mailto:bsskra@bath.ac.uk); Fax: (+44) 1225-386779

### Authors

Urvashi Sharma – Department of Biology and Biochemistry, University of Bath, Bath BA2 7AY, United Kingdom

Gyles E. Cozier – Department of Biology and Biochemistry, University of Bath, Bath BA2 7AY, United Kingdom

Edward D. Sturrock – Department of Integrative Biomedical Sciences, Institute of Infectious Disease and Molecular Medicine, University of Cape Town, 7935 Cape Town, Republic of South Africa

Complete contact information is available at:

<https://pubs.acs.org/doi/10.1021/acs.jmedchem.0c00441>

### Author Contributions

§U.S. and G.E.C. contributed equally to this work.

### Author Contributions

U.S. performed protein expression, purification, produced the crystals, collected the data, and contributed to the manuscript. G.E.C. processed, refined, and analyzed the X-ray data and wrote the manuscript. E.D.S. edited the manuscript. K.R.A. supervised the study, analyzed the data, and edited the manuscript. All authors reviewed the manuscript.

### Notes

The authors declare no competing financial interest.

## ■ ACKNOWLEDGMENTS

The authors thank the scientists at station i04 (Proposal Number mx17212) of Diamond Light Source, Didcot, Oxfordshire (U.K.), for their support during X-ray diffraction data collection. This work was supported by the Medical Research Council (U.K.) Project Grant MR/M026647/1 (to K.R.A.) and the National Research Foundation (South Africa)

CPRR grant 13082029517 (to E.D.S.). K.R.A. and E.D.S. also thank the University of Cape Town (South Africa) and University of Bath (U.K.), respectively, for the Visiting Professorship.

## ■ ABBREVIATIONS USED

ACE, angiotensin-I-converting enzyme; AnCE, drosophila ACE homologue; BK, bradykinin; BPP, bradykinin-potentiating peptide; cACE, ACE C-domain; FII, phosphinic tripeptide; nACE, ACE N-domain; NEP, neprilysin; RAAS, renin–angiotensin–aldosterone system; sACE, somatic ACE; tACE, testis ACE; Z-FHL, Cbz-Phe-His-Leu

## ■ REFERENCES

- (1) Egan, B. M.; Kjeldsen, S. E.; Grassi, G.; Esler, M.; Mancia, G. The global burden of hypertension exceeds 1.4 billion people: should a systolic blood pressure target below 130 become the universal standard? *J. Hypertens.* **2019**, *37*, 1148–1153.
- (2) Nussberger, J.; Cugno, M.; Amstutz, C.; Cicardi, M.; Pellacani, A.; Agostoni, A. Plasma bradykinin in angio-oedema. *Lancet* **1998**, *351*, 1693–1697.
- (3) Steckelings, U. M.; Artuc, M.; Wollschlager, T.; Wiehstutz, S.; Henz, B. M. Angiotensin-converting enzyme inhibitors as inducers of adverse cutaneous reactions. *Acta Derm.-Venereol.* **2001**, *81*, 321–325.
- (4) Weber, M. A.; Messerli, F. H. Angiotensin-converting enzyme inhibitors and angioedema: estimating the risk. *Hypertension* **2008**, *51*, 1465–1467.
- (5) Arendse, L. B.; Danser, A. H. J.; Poglitsch, M.; Touyz, R. M.; Burnett, J. C., Jr; Llorens-Cortes, C.; Ehlers, M. R.; Sturrock, E. D. Novel therapeutic approaches targeting the renin-angiotensin system and associated peptides in hypertension and heart failure. *Pharmacol. Rev.* **2019**, *71*, 539–570.
- (6) Nathisuwan, S.; Talbert, R. L. A review of vasopeptidase inhibitors: a new modality in the treatment of hypertension and chronic heart failure. *Pharmacotherapy* **2002**, *22*, 27–42.
- (7) Trindade, P. T.; Rouleau, J. L. Vasopeptidase inhibitors: potential role in the treatment of heart failure. *Heart Failure Monit.* **2001**, *2*, 2–7.
- (8) Weber, M. A. Vasopeptidase inhibitors. *Lancet* **2001**, *358*, 1525–1532.
- (9) Cozier, G. E.; Arendse, L. B.; Schwager, S. L.; Sturrock, E. D.; Acharya, K. R. Molecular basis for multiple omapatrilat binding sites within the ACE C-domain: Implications for drug design. *J. Med. Chem.* **2018**, *61*, 10141–10154.
- (10) Robl, J. A.; Sun, C. Q.; Stevenson, J.; Ryono, D. E.; Simpkins, L. M.; Cimarusti, M. P.; Dejneka, T.; Slusarchyk, W. A.; Chao, S.; Stratton, L.; Misra, R. N.; Bednarz, M. S.; Asaad, M. M.; Cheung, H. S.; Abboa-Offei, B. E.; Smith, P. L.; Mathers, P. D.; Fox, M.; Schaeffer, T. R.; Seymour, A. A.; Trippodo, N. C. Dual metalloprotease inhibitors: mercaptoacetyl-based fused heterocyclic dipeptide mimetics as inhibitors of angiotensin-converting enzyme and neutral endopeptidase. *J. Med. Chem.* **1997**, *40*, 1570–1577.
- (11) Azizi, M.; Massien, C.; Michaud, A.; Corvol, P. In vitro and in vivo inhibition of the 2 active sites of ACE by omapatrilat, a vasopeptidase inhibitor. *Hypertension* **2000**, *35*, 1226–1231.
- (12) Kostis, J. B.; Packer, M.; Black, H. R.; Schmieder, R.; Henry, D.; Levy, E. Omapatrilat and enalapril in patients with hypertension: the Omapatrilat Cardiovascular Treatment vs. Enalapril (OCTAVE) trial. *Am. J. Hypertens.* **2004**, *17*, 103–111.
- (13) Fryer, R. M.; Segreti, J.; Banfor, P. N.; Widomski, D. L.; Backes, B. J.; Lin, C. W.; Ballaron, S. J.; Cox, B. F.; Trevillyan, J. M.; Reinhart, G. A.; von Geldern, T. W. Effect of bradykinin metabolism inhibitors on evoked hypotension in rats: rank efficacy of enzymes associated with bradykinin-mediated angioedema. *Br. J. Pharmacol.* **2008**, *153*, 947–955.

- (14) Kirk, J. E.; Wilkins, M. R. Renal effects of concurrent E-24.11 and ACE inhibition in the aorto-venocaval fistula rat. *Br. J. Pharmacol.* **1996**, *119*, 943–948.
- (15) Sharma, R. K.; Espinoza-Moraga, M.; Poblete, H.; Douglas, R. G.; Sturrock, E. D.; Caballero, J.; Chibale, K. The dynamic nonprime binding of sampatrilat to the C-domain of angiotensin-converting enzyme. *J. Chem. Inf. Model.* **2016**, *56*, 2486–2494.
- (16) Venn, R. F.; Barnard, G.; Kaye, B.; Macrae, P. V.; Saunders, K. C. Clinical analysis of sampatrilat, a combined renal endopeptidase and angiotensin-converting enzyme inhibitor II: assay in the plasma and urine of human volunteers by dissociation enhanced lanthanide fluorescence immunoassay (DELFLIA). *J. Pharm. Biomed. Anal.* **1998**, *16*, 883–892.
- (17) Venn, R. F.; Kaye, B.; Macrae, P. V.; Saunders, K. C. Clinical analysis of sampatrilat, a combined renal endopeptidase and angiotensin-converting enzyme inhibitor I: assay in plasma of human volunteers by atmospheric-pressure ionisation mass-spectrometry following derivatisation with BF<sub>3</sub>-methanol. *J. Pharm. Biomed. Anal.* **1998**, *16*, 875–881.
- (18) Wallis, E. J.; Ramsay, L. E.; Hettiarachchi, J. Combined inhibition of neutral endopeptidase and angiotensin-converting enzyme by sampatrilat in essential hypertension. *Clin. Pharmacol. Ther.* **1998**, *64*, 439–449.
- (19) Watermeyer, J. M.; Kroger, W. L.; O'Neill, H. G.; Sewell, B. T.; Sturrock, E. D. Characterization of domain-selective inhibitor binding in angiotensin-converting enzyme using a novel derivative of lisinopril. *Biochem. J.* **2010**, *428*, 67–74.
- (20) Burger, D.; Reudelhuber, T. L.; Mahajan, A.; Chibale, K.; Sturrock, E. D.; Touyz, R. M. Effects of a domain-selective ACE inhibitor in a mouse model of chronic angiotensin II-dependent hypertension. *Clin. Sci.* **2014**, *127*, 57–63.
- (21) Deddish, P. A.; Marcic, B.; Jackman, H. L.; Wang, H. Z.; Skidgel, R. A.; Erdos, E. G. N-domain-specific substrate and C-domain inhibitors of angiotensin-converting enzyme: angiotensin-(1-7) and keto-ACE. *Hypertension* **1998**, *31*, 912–917.
- (22) Sharp, S.; Poglitsch, M.; Zilla, P.; Davies, N. H.; Sturrock, E. D. Pharmacodynamic effects of C-domain-specific ACE inhibitors on the renin-angiotensin system in myocardial infarcted rats. *J. Renin-Angiotensin-Aldosterone Syst.* **2015**, *16*, 1149–1158.
- (23) Cozier, G. E.; Schwager, S. L.; Sharma, R. K.; Chibale, K.; Sturrock, E. D.; Acharya, K. R. Crystal structures of sampatrilat and sampatrilat-Asp in complex with human ACE - a molecular basis for domain selectivity. *FEBS J.* **2018**, *285*, 1477–1490.
- (24) Labiuk, S. L.; Sygusch, J.; Grochulski, P. Structures of soluble rabbit neprilysin complexed with phosphoramidon or thiorphan. *Acta Crystallogr., Sect. F: Struct. Biol. Commun.* **2019**, *75*, 405–411.
- (25) Oefner, C.; D'Arcy, A.; Hennig, M.; Winkler, F. K.; Dale, G. E. Structure of human neutral endopeptidase (Neprilysin) complexed with phosphoramidon. *J. Mol. Biol.* **2000**, *296*, 341–349.
- (26) Schiering, N.; D'Arcy, A.; Villard, F.; Ramage, P.; Logel, C.; Cumin, F.; Ksander, G. M.; Wiesmann, C.; Karki, R. G.; Mogi, M. Structure of neprilysin in complex with the active metabolite of sacubitril. *Sci. Rep.* **2016**, *6*, No. 27909.
- (27) Griggs, D. W.; Prinsen, M. J.; Oliva, J.; Campbell, M. A.; Arnett, S. D.; Tajfrouz, D.; Ruminski, P. G.; Yu, Y.; Bond, B. R.; Ji, Y.; Neckermann, G.; Choy, R. K.; de Hostos, E.; Meyers, M. J. Pharmacologic comparison of clinical neutral endopeptidase inhibitors in a rat model of acute secretory diarrhea. *J. Pharmacol. Exp. Ther.* **2016**, *357*, 423–431.
- (28) Kukkola, P. J.; Savage, P.; Sakane, Y.; Berry, J. C.; Bilci, N. A.; Ghai, R. D.; Jeng, A. Y. Differential structure-activity relationships of phosphoramidon analogues for inhibition of three metalloproteases: endothelin-converting enzyme, neutral endopeptidase, and angiotensin-converting enzyme. *J. Cardiovasc. Pharmacol.* **1995**, *26*, S65–S68.
- (29) Gaucher, J. F.; Selkti, M.; Tiraboschi, G.; Prange, T.; Roques, B. P.; Tomas, A.; Fournie-Zaluski, M. C. Crystal structures of alpha-mercaptoacyldipeptides in the thermolysin active site: structural parameters for a Zn monodentation or bidentation in metalloendopeptidases. *Biochemistry* **1999**, *38*, 12569–12576.
- (30) Ksander, G. M.; de Jesus, R.; Yuan, A.; Ghai, R. D.; McMartin, C.; Bohacek, R. Meta-substituted benzofused macrocyclic lactams as zinc metalloprotease inhibitors. *J. Med. Chem.* **1997**, *40*, 506–514.
- (31) Ksander, G. M.; de Jesus, R.; Yuan, A.; Ghai, R. D.; Trapani, A.; McMartin, C.; Bohacek, R. Ortho-substituted benzofused macrocyclic lactams as zinc metalloprotease inhibitors. *J. Med. Chem.* **1997**, *40*, 495–505.
- (32) Tiraboschi, G.; Jullian, N.; They, V.; Antonczak, S.; Fournie-Zaluski, M. C.; Roques, B. P. A three-dimensional construction of the active site (region 507-749) of human neutral endopeptidase (EC.3.4.24.11). *Protein Eng., Des. Sel.* **1999**, *12*, 141–149.
- (33) Jaspard, E.; Wei, L.; Alhenc-Gelas, F. Differences in the properties and enzymatic specificities of the two active sites of angiotensin I-converting enzyme (kininase II). Studies with bradykinin and other natural peptides. *J. Biol. Chem.* **1993**, *268*, 9496–9503.
- (34) Corradi, H. R.; Chitapi, I.; Sewell, B. T.; Georgiadis, D.; Dive, V.; Sturrock, E. D.; Acharya, K. R. The structure of testis angiotensin-converting enzyme in complex with the C-domain specific inhibitor RXPA380. *Biochemistry* **2007**, *46*, 5473–5478.
- (35) Jullien, N.; Makritis, A.; Georgiadis, D.; Beau, F.; Yiotakis, A.; Dive, V. Phosphinic tripeptides as dual angiotensin-converting enzyme C-domain and endothelin-converting enzyme-1 inhibitors. *J. Med. Chem.* **2010**, *53*, 208–220.
- (36) Moss, S.; Subramanian, V.; Acharya, K. R. High resolution crystal structure of substrate-free human neprilysin. *J. Struct. Biol.* **2018**, *204*, 19–25.
- (37) Waterman, D. G.; Winter, G.; Gildea, R. J.; Parkhurst, J. M.; Brewster, A. S.; Sauter, N. K.; Evans, G. Diffraction-geometry refinement in the DIALS framework. *Acta Crystallogr., Sect. D: Struct. Biol.* **2016**, *72*, 558–575.
- (38) Evans, P. R.; Murshudov, G. N. How good are my data and what is the resolution? *Acta Crystallogr., Sect. D: Biol. Crystallogr.* **2013**, *69*, 1204–1214.
- (39) Collaborative Computational Project Number 4. The CCP4 suite: programs for protein crystallography. *Acta Crystallogr., Sect. D: Biol. Crystallogr.* **1994**, *50*, 760–763.
- (40) McCoy, A. J.; Grosse-Kunstleve, R. W.; Adams, P. D.; Winn, M. D.; Storoni, L. C.; Read, R. J. Phaser crystallographic software. *J. Appl. Crystallogr.* **2007**, *40*, 658–674.
- (41) Murshudov, G. N.; Vagin, A. A.; Dodson, E. J. Refinement of macromolecular structures by the maximum-likelihood method. *Acta Crystallogr., Sect. D: Biol. Crystallogr.* **1997**, *53*, 240–255.
- (42) Adams, P. D.; Afonine, P. V.; Bunkoczi, G.; Chen, V. B.; Davis, I. W.; Echols, N.; Headd, J. J.; Hung, L. W.; Kapral, G. J.; Grosse-Kunstleve, R. W.; McCoy, A. J.; Moriarty, N. W.; Oeffner, R.; Read, R. J.; Richardson, D. C.; Richardson, J. S.; Terwilliger, T. C.; Zwart, P. H. PHENIX: a comprehensive Python-based system for macromolecular structure solution. *Acta Crystallogr., Sect. D: Biol. Crystallogr.* **2010**, *66*, 213–221.
- (43) Emsley, P.; Cowtan, K. Coot: model-building tools for molecular graphics. *Acta Crystallogr., Sect. D: Biol. Crystallogr.* **2004**, *60*, 2126–2132.
- (44) Chen, V. B.; Arendall, W. B., III; Headd, J. J.; Keedy, D. A.; Immormino, R. M.; Kapral, G. J.; Murray, L. W.; Richardson, J. S.; Richardson, D. C. MolProbity: all-atom structure validation for macromolecular crystallography. *Acta Crystallogr., Sect. D: Biol. Crystallogr.* **2010**, *66*, 12–21.
- (45) McNicholas, S.; Potterton, E.; Wilson, K. S.; Noble, M. E. Presenting your structures: the CCP4mg molecular-graphics software. *Acta Crystallogr., Sect. D: Biol. Crystallogr.* **2011**, *67*, 386–394.
- (46) Laskowski, R. A.; Swindells, M. B. LigPlot+: multiple ligand-protein interaction diagrams for drug discovery. *J. Chem. Inf. Model.* **2011**, *51*, 2778–2786.